CONF-900801--33

Effects of Jet Port Arrangement on Three-Dimensional Non-Reacting Jet-Gas Mixing in an MHD Second Stage Combustor

CONF-900801--33

DE90 017858

DISCLAIMER

S.A. Lottes, S.L. Chang, and G.F. Berry

Energy Systems Division
Argonne National Laboratory
9700 South Cass Avenue
Argonne, Illinois 60439

Manuscript submitted to
The 25th Intersociety Energy Conversion Engineering Conference
August 12-18, 1990
Reno, Nevada

Effects of Jet Port Arrangement on Three-Dimensional Non-Reacting Jet-Gas Mixing in an MHD Second Stage Combustor

S.A. Lottes, S.L. Chang and G.F. Berry
Argonne National Laboratory
9700 South Cass Avenue
Argonne, Illinois 60439

ABSTRACT

A three-dimensional hydrodynamics computer code was used to investigate the flow mixing processes in an MHD second stage combustor. The code solves the conservation equations of mass, momentum, energy, and a transport equation of turbulence kinetic energy. The flow mixing patterns of four different jet port arrangements, including a 12-jet, an 8-center-jet, an 8-side-jet, and an 8-mixed-jet (4 side and 4 center jets), were computed and compared. Jet and gas seems to mix in two stages: an early and more effective convective stage and a later diffusive stage. For the same bulk jet concentration, the 12-jet arrangement has better jet-gas mixing than the other three 8-jet arrangements.

NOMENCLATURE

A	Cross-sectional area in Y-Z plane (m^2)
D	Combustor width (m)
k	Turbulent kinetic energy (J/kg)
H	Combustor height (m)
h	Enthalpy (J/kg)
L	Combustor length (m)
L_j	Jet port location in X-coordinate (m)
S	Source terms in conservation equations
T	Temperature (K)
u	Velocity (m/s)
X	Displacement coordinate (m)
Y	Displacement coordinate (m)
Z	Displacement coordinate (m)

Greek Letters

ϕ	General dependent variable
Γ	Diffusion coefficient (turbulent and laminar)
ρ	Density (kg/m^3)
σ	Normalized cross-sectional temperature deviation
τ	Average cross-sectional temperature (K)

Subscripts

i,j	Summation index

INTRODUCTION

Magnetohydrodynamics (MHD) power generation can attain higher overall efficiency and produce less air pollution than conventional coal-fired power plants [1]. The Department of Energy has been sponsoring the national coal-fired MHD development program including the development of a prototype 50 MWt coal-fired MHD combustor at TRW [2]. The coal-fired combustor (CFC) uses two-stage combustion processes to achieve design criteria: high electrical conductivity, high slag recovery, low heat loss, low unburned carbon carry-over, and stable combustion. In the first stage, pulverized coal is burned sub-stoichiometrically in a highly swirling preheated air stream to remove slag and maintain stable combustion. In the second stage, additional oxygen is injected to mix with the first stage combustion products and the mixture is burned to a high gas temperature. Tests have been performed to evaluate the effects of the non-uniformity of mixture temperature and velocity in the second stage combustor on the MHD channel performance. Poor jet penetration and jet-gas mixing are believed to be mainly responsible for the non-uniformity. Good mixing between the first stage sub-stoichiometric combustion products (or gas flow) and the oxidizer jets (or jet flow) would promote more uniform and complete combustion in the second stage [3,4].

Holdeman and Walker [5] and Rudinger [6] developed empirical models to predict penetration and mixing characteristics of jets in a confined crossflow based on experimental data and a self-similar flow principle. Scaling parameters like momentum flux ratio, mass ratio, and density were used to correlate the penetration and mixing parameters. In recent years, some numerical solutions of the deflected-jet situations have been reported. Patankar, Basu, and Alpay [7] used a comprehensive three-dimensional turbulent flow computer model and predicted the velocity field generated by a round jet deflected by a main stream normal to the jet axis with some success.

Argonne National Laboratory (ANL) uses a two-dimensional combustion computer code and a three-dimensional hydrodynamics computer code to investigate the flow mixing and combustion processes in an MHD second stage combustor. The two-dimensional combustion code is used to simulate the two-fluid mixing and combustion processes and the three-dimensional code is used to study non-reacting jet penetration and jet-gas mixing patterns. At the present stage, ANL's investigation covers the non-reacting flow mixing simulations. This paper presents some results computed using the three-dimensional hydrodynamic code and compares the mixing patterns of four different jet port arrangements.

COMPUTATIONAL APPROACH

The COMMIX code, previously developed at ANL [8], solves the conservation equations of mass, momentum, energy, and a transport equation of a turbulence parameter. The conservation equations possess a common form. If one denotes the general dependent variable ϕ to represent a scalar 1 in the continuity equation, three velocity components, u_i, i=1, 2, and 3, in momentum equations, enthalpy, h, in energy equation, and turbulent kinetic energy, k, in a one-parameter turbulence model, the conservation equations have the following form in Cartesian coordinate system.

$$\partial(\rho u_j \phi)/\partial X_j = \partial(\Gamma_\phi \partial\phi/\partial X_i)/\partial X_i + S_\phi$$

Inlet conditions are specified by the user. Walls are treated as adiabatic, and wall functions are used to bridge the near wall boundary layer. The equations are solved by using a fully implicit algorithm in a staggered grid system. The details of the COMMIX code are described in reference 8.

Two different fluids (gas and jet) are mixed in the combustor. The COMMIX code can treat only one fluid in its solution procedure. Flows of two different temperatures are chosen to represent gas and jet flows. The enthalpy (or temperature) of a computational cell is effectively an average of the enthalpies of both jet and gas flows in the cell on a mass basis. If the jet temperature is higher than the gas temperature, the mass fraction of the jet flow in a cell is primarily proportional to the temperature rise.

An important feature of COMMIX code is that it allows the users to specify permeable surfaces for a computational cell. To allow jet penetration in a cross-stream direction in a computer simulation, a jet entry model was developed. The jet entry model uses a one-cell non-permeable channel next to the injection port for each jet entry. The entry channel consists of four one-cell nonpermeable surfaces perpendicular to the jet flow direction and a partially permeable surface on the end of the channel. The jet entry model allows the jet to be injected into the cross-stream flow with a specified velocity, controlled by the surface permeability of the entry channel. The COMMIX code with this jet entry model was tested by comparing with a two-dimensional combustion computer code. The results showed good agreement.

Statistical parameters are used for comparing the degree of mixing between gas and jet flows under various conditions. For a Y-Z cross-section, the average temperature is,

$$\tau(X) = \iint T\, dA / A$$

and the normalized temperature deviation is defined as,

$$\sigma(X) = [\iint (T - \tau)^2\, dA / A]^{1/2} / \tau$$

In general, the lower the temperature deviation the better the mixing. If the flows are perfectly mixed, the average temperature is the bulk temperature and the temperature deviation becomes zero.

JET PORT ARRANGEMENTS

Figure 1 shows an idealized CFC second stage combustor under investigation; it consists of four solid side walls (front, back, top, and bottom), an inlet (left), and an exit (right). The first stage sub-stoichiometric coal combustion products (gas flow) enters the second stage combustor through the inlet to mix with additional oxidizer (jet flow) and complete the combustion. There are opposing jet ports on top and bottom walls. The 12-jet arrangement has 6 evenly spacing jet ports, T1, T2, T3, T4, T5, and T6 on the top wall and 6 opposing jet ports, B1, B2, B3, B4, B5, and B6 on the bottom wall, as shown in Figure 2. There are three 8-jet arrangements derived from the 12-jet arrangement: 8-center, 8-side and 8-mixed. The 8-center-jet arrangement deletes two pairs of jet ports T1, B1, T6, and B6; the 8-side-jet deletes T3, B3, T4, and B4; the 8-mixed-jet (or 4-side-4-center-jet) deletes T2, B2, T5, and B5. Combustor geometry and simulation flow conditions are summarized in Table I.

Table I Combustor Geometry and Flow Conditions

Combustor Dimension (L:D:H) =	3.8:1:1
Jet Port Location (L_j/D) =	0.66
Pressure =	1 atm
Inlet Gas Velocity =	23 m/s
Bulk Jet Concentration =	6.4 %
Jet Angle =	90 deg.

The coordinate origin is set at the lower left corner of the inlet plane with X-, Y- and Z-axes in main flow, width, and height directions, as shown in Figure 1. A 41 by 21 by 13 grid system

is defined for the computational domain of this geometry. For a symmetrical arrangement, only 41 by 11 by 7 nodes are used in the computation. Computation of a symmetrical case with good numerical convergence generally requires about 1600 seconds of CPU time on a CRAY/XMP supercomputer.

RESULTS AND DISCUSSION

Analysis of results focuses on the effects of the jet port arrangement and jet velocity on thermal mixing. The development of mixing patterns is presented in the form of contour plots of normalized temperature difference at four X-direction positions downstream of the injectors. Normalized temperature difference is defined as,

$$\beta = (T - T_{gas})/(\tau - T_{gas})$$

where T_{gas} is the inlet gas temperature.

Two cases of interest used all 12 jets, but different jet injection velocities. The first test case employed all 12 jets with a high jet velocity (614 m/s). In this case jet momentum is sufficient for the opposing jets to impinge in the center of the channel. Spikes of hot jet fluid in route to channel center are clearly visible in Figure 3a. Further downstream, the jets have impinged forming sandwiched layers of hot and cold fluid, Figure 3b. This layering increases the interface area between hot and cold fluid, promoting thermal mixing. Because the jet distribution is evenly spaced across the Z coordinate, the sandwich pattern tends to persist into the downstream, see Figures 3c and 3d. The second case also employed all 12 jets, but the jet velocity was lower (307 m/s). When jet momentum is insufficient for the jets to penetrate to chamber center, a thick layer of cold gas fluid occupies the mid-section of the Y coordinate as shown in Figures 4a and 4b. In this case, jets have been turned into the downstream before reaching the mid-plane of the Y coordinate, and jet penetration toward the Y coordinate mid-plane occurs primarily through turbulent diffusion, a relatively slow process compared to the convective mixing near jet entries. As a consequence of this limited mixing pattern a zone of only cold gas fluid persists to the end of the chamber, Figures 4c and 4d.

Three arrangements of eight jet ports on the top and bottom walls were investigated. These arrangements employed uneven jet spacing created by deleting a corresponding pair of jets from each wall of the 12 port arrangement. Deleting pairs of jets as described under Jet Port Arrangement, creates larger gaps either between jets or between jet and wall. The gaps where the jets were deleted provide zones where the remaining impinging jets can spread out in the horizontal or Z direction. This spreading may create secondary flows or vortices in the Y-Z plane. A question of considerable importance in this study was whether the secondary flows created by uneven jet spacing would enhance the thermal mixing, and if so which of the arrangements tested would produce the best mixing.

The temperature contours for the case of 4-side and 4-center jets are shown in Figure 5. To produce the same mass flow rate as in the high velocity 12-jet injection case, a higher jet velocity was used (921 m/s). With this jet velocity, jet impingement at the central X-Z plane has already occurred by X/D = 1, Figure 5a. The gap between jets 1 and 3 and jets 4 and 6, allows the hot jet fluid to spread out in the Z direction after impingement to form a thin layer of hot fluid at the mid point of the Y coordinate, Figure 5b. The fluid spreading horizontally in the chamber center as a result of opposing jet impingement also spreads in opposing directions in the gap between jets. Thus, near the midpoint of the gap the secondary flow must turn again forming four recirculation zones. The deformation of the temperature contours due to this developing recirculation in the Y-Z plane can be seen in Figures 5b, 5c, and 5d. The recirculation does fold hot layers of fluid against colder layers, but this layering occurs primarily only around the vertical line through the chamber center.

With 8 jets centrally configured, the wide gaps where jets were deleted lie between the walls and the remaining jets. In this configuration, the impingement of jets configured on either side of the chamber center forms a hot spot in the center, Figure 6a. The hot spot spreads out in a hot horizontal layer toward the side walls, Figure 6b. The absence of jets near the side walls allows a secondary flow to develop from center to side walls. Upon nearing the wall midpoint, the secondary flow splits and follows the wall around until it meets at the upper and lower wall midpoint and turns back toward the chamber center. Thus, four vortices are formed in the Y-Z plane that circulate hot fluid out from the center to the side wall regions. The colder fluid in the upper and lower regions of the chamber is folded in on itself and pushed toward the chamber center as the hot fluid spreads out along the side walls, Figures 6b and 6c. This circulation pattern does not create zones where hot fluid is extended into zones in close proximity to the colder portions of the main gas flow. The hottest and coldest fluid come into close proximity only in the central region where interface area between hottest and coldest fluid is relatively small, as colder fluid pushes into the center pinching off the hot layer as it moves out against the side walls, Figures 6b and 6c. At the chamber exit, the positions of hottest and coldest fluid have nearly reversed. The cold spot at the exit plane is in the chamber center, Figure 6d.

The configuration of 8 jets with gap in the center, referred to as side jets, produces recirculation zones with an opposite sense of rotation to that of the central jets configuration. In the case of side jets, hot fluid from impinging jets spreads out toward the center, Figure 7a, producing a hot horizontal layer at the center, Figure 7b. The opposing flow of

hot fluid from sides into center causes hot fluid building up in the center to bulge up toward the top and bottom walls, Figure 7c. These hot bulges cause the cold fluid to fold in on itself along the upper side walls in the four corner quadrants, Figure 7d. The development of the rotation in this case is slower than for the central jet configuration due to reduction of jet momentum through drag induced by interaction with the side walls.

The normalized temperature deviation (σ) over a chamber cross section is used to quantify the degree of mixing between jet and gas streams. The development of jet and gas stream mixing as the flow moves down the chamber for the 12-jet impinging and non-impinging arrangements and the various 8-jet arrangements is plotted in terms of temperature deviation in Figure 8. All cases show a region of rapid convective mixing where the jets are penetrating the gas flow just downstream of the injectors. Once the jets have been turned into the downstream, mixing is slower and depends primarily on turbulent transport and diffusion between neighboring layers of cold and hot fluid. The 8-jet arrangements all have a more rapid initial mixing rate than the 12-jet cases because the 8-jet injection velocity was 50 percent higher (to make 8 and 12 port injection mass flow rates the same) giving the 8 port jets a deeper penetration into the gas flow than the 12 port jets. In the downstream, however, the mixing in the 12 port arrangement with jet impingement overtakes all of the 8 port arrangements due to the sustained pattern of many alternating columns of hot and cold fluid yielding the highest overall temperature gradient field which in turn yields a higher rate of turbulent and diffusive mixing. The 8-mixed-jet case gives the highest mixing rate among the 8-jet arrangements primarily because the 4-side-4-center arrangement provides more hot jet to cold gas flow interface area than the central or side jet arrangements. The side and central 8-jet configurations promote secondary flow vortices in the Y-Z plane, but these vortices do not give these configurations a mixing advantage over the 4-side-4-center-jet configuration or the 12-impinging-jet configuration because the vortices primarily rotate the thermal layers around without stretching and folding hot against cold layer to any significant degree. The case of 12 port nonimpinging jets clearly gives a slower mixing rate than any of the other cases.

CONCLUSION

A three-dimensional hydrodynamics computer code was used to investigate the flow mixing processes in an MHD second stage combustor. The flow and mixing patterns of four different jet port arrangements, including a 12-jet, an 8-center-jet, an 8-side-jet, and an 8-mixed-jet, were computed and compared. Jet and gas mixing is found to happen in two stages: an early convective stage and a later diffusive stage. Convective mixing is much more effective than diffusive mixing. A nonimpinging 12-jet arrangement has poor mixing. For the same bulk jet concentration, the 12-jet arrangement has better jet-gas mixing than the other three 8-jet arrangements. Between the three 8-jet arrangements, the 4-side-4-center jets mix better with the main gas flow.

ACKNOWLEDGEMENTS

This work is supported by U.S. Department of Energy, Assistant Secretary for Fossil Energy, under Contract W-31-109-ENG-38. Mr. Paul Lissak is appreciated for his assistance in preparing the figures.

REFERENCES

[1] "Open-Cycle Magnetohydrodynamic Electric Power generation, M. Petrick and B. Ya. Shumyatsky, eds., joint report of Argonne National Laboratory and U.S.S.R. Academy of Science (1978).

[2] Listvinsky, G., J. Alpay, L. Hil, K. King, D. Paul, D. Vanevenhoven, K. Natesan and D.Y. Wang "Development of a Prototypical MHD Coal Combustor," Proc. of 24th Intersociety Energy Conversion Engineering Conference, Washington, D.C., 2:965-970 (August 6-11, 1989).

[3] McClaine, A., J. Pinsley, and B. Pote, "Experimental Investigation on the Effects of the TRW Two-Stage Coal Combustor on the Performance of the AVCO Mk VI MHD Generator," Proc. of 24th Intersociety Energy Conversion Engineering Conference, Washington, D.C., 2:971-977 (August 6-11, 1989).

[4] Burkhart, T., G. Funk, R. Glovan, A. Hart, A. Herbst, J. Joyce, Y.M. Lee, S. Lundberg, and I. Stepan, "Coal-Fired MHD Topping Cycle Hardware and Test Progress at the Component Development and Integration Facility," Proc. of 23rd Intersociety Energy Conversion Engineering Conference, Denver, CO, 4:445-453, (July 31-August 5, 1988).

[5] Holdeman, J.D., and R.E. Walker, "Mixing of a Row of Jets with a Confined Crossflow," AIAA Journal, Vol. 15, No. 2, pp. 243-249, (1977).

[6] Rudinger, G., "Experimental Investigation of Gas Injection through a Transverse Slot into a Subsonic Cross Flow," AIAA Journal Vol. 12, No. 4, pp. 566-568 (1973).

[7] Patankar, S.V., D.K. Basu, and S.A. Alpay, "Prediction of the Three-Dimensional Velocity Field of a Deflected Turbulent Jet," Tran. of ASME, pp. 758-762 (Dec. 1977).

[8] Domanus, H.M., R.C. Schmitt, W.T. Sha, and V.L. Shah, "COMMIX-1A: A Three-Dimensional Transient Single-Phase Computer Program for Thermal Hydraulic Analysis of Single and Multicomponents Systems," NUREG/CR-2896, ANL-82-25 (1983).

FIGURES:

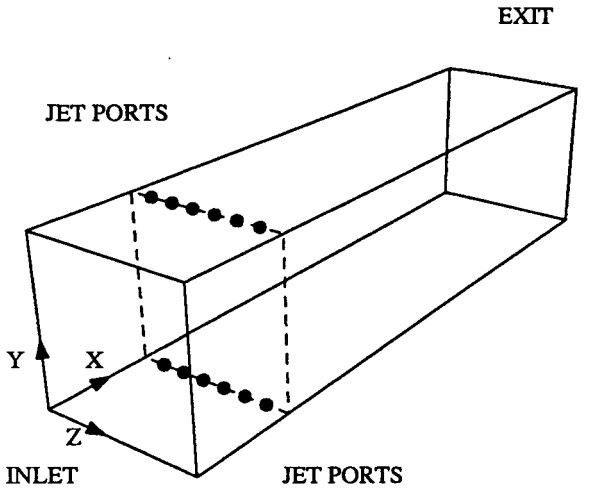

Figure 1 Idealized MHD second stage combustor geometry

(a) Top wall

(b) Bottom wall

Figure 2 Jet port locations

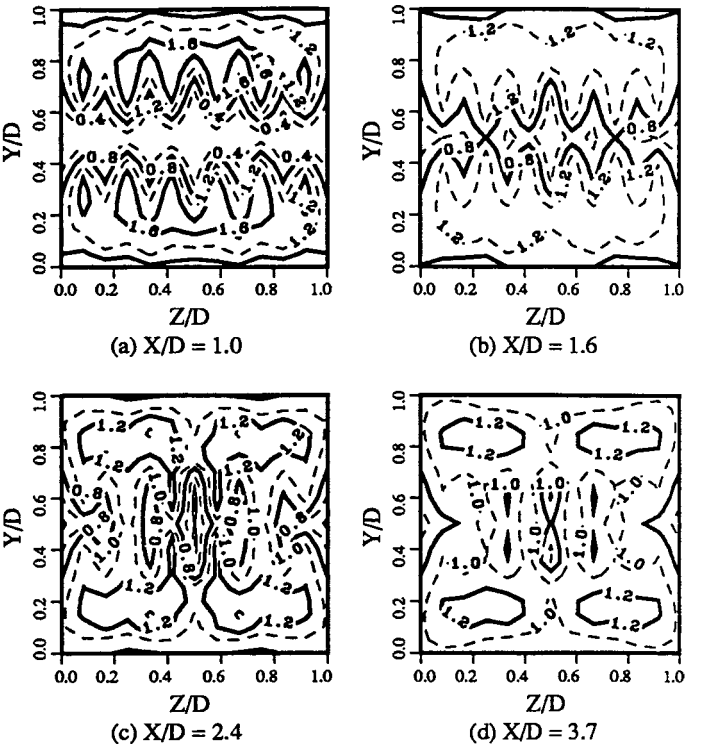

Figure 3 Development of thermal mixing
(βcontours, 12-impinging-jet)

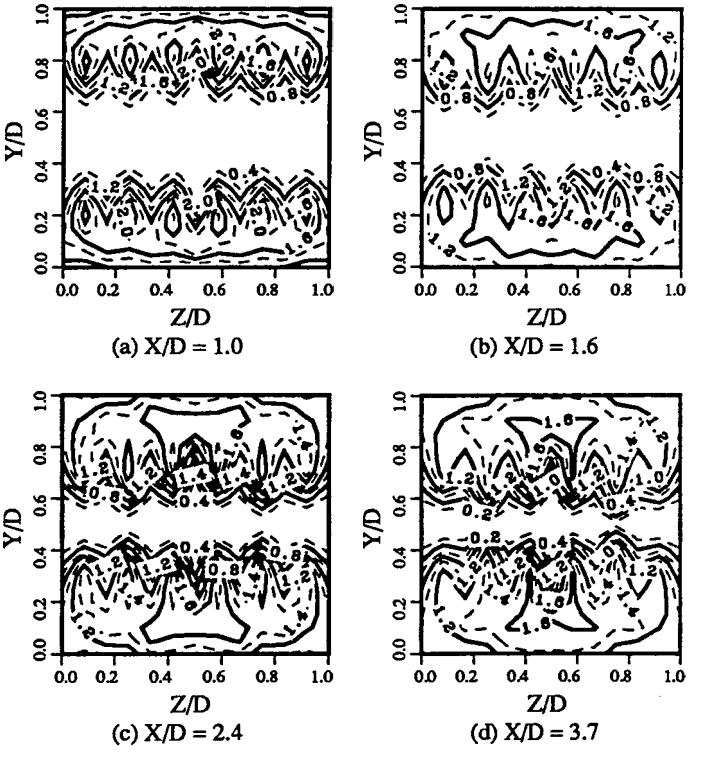

Figure 4 Development of thermal mixing
(βcontours, 12-nonimpinging-jet)

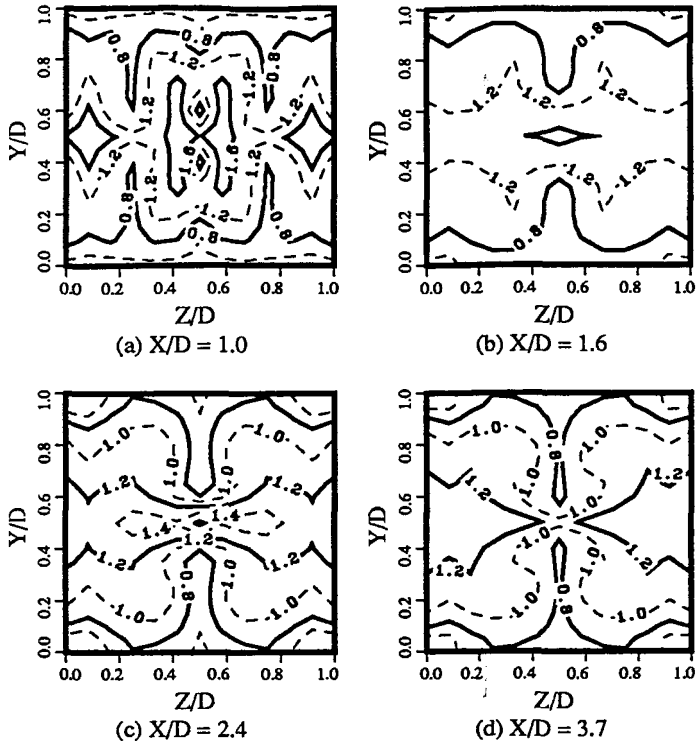

Figure 5 Development of thermal mixing
(β contours, 4-side-4-center-jet)

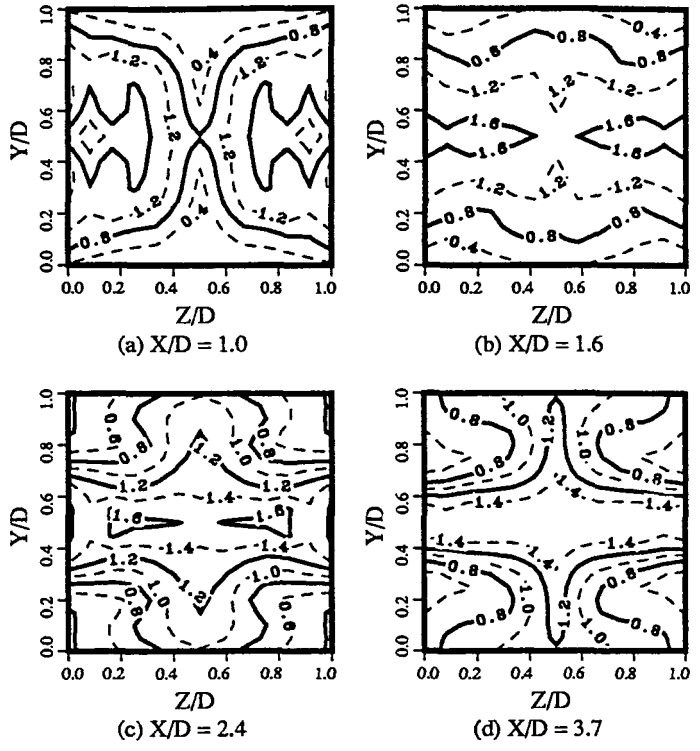

Figure 7 Development of thermal mixing
(β contours, 8-side-jet)

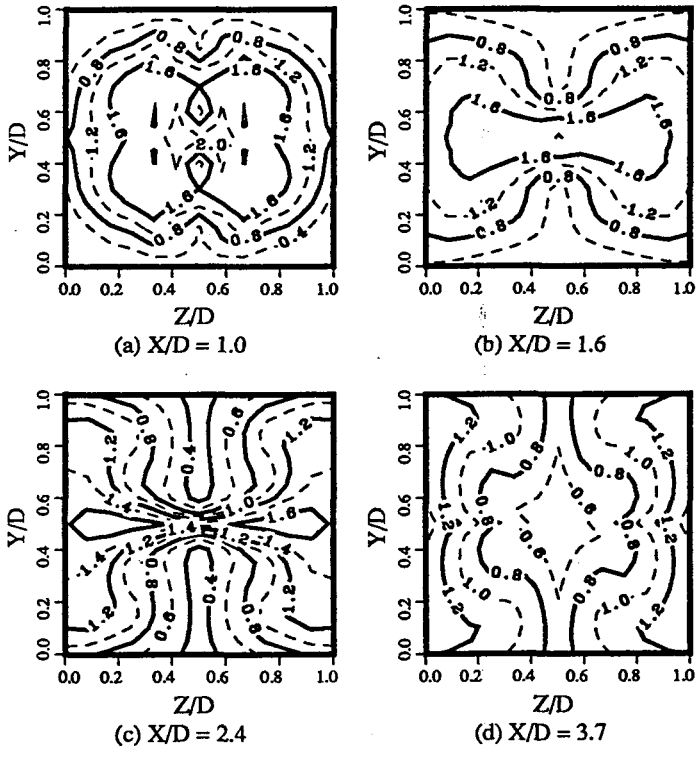

Figure 6 Development of thermal mixing
(β contours, 8-center-jet)

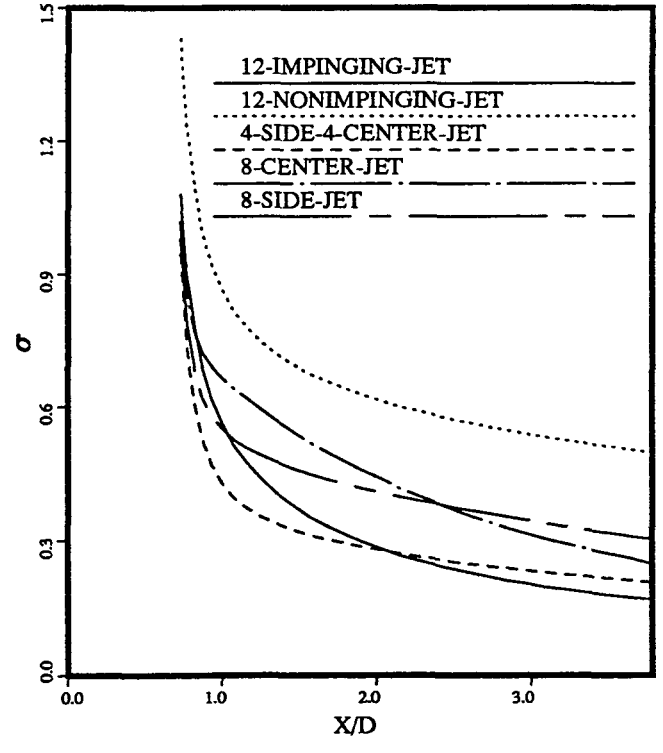

Figure 8 Comparison of thermal mixing